Inorg. Chem. **2007**, *46*, 3236–3244

Cyano-Bridged $Fe^{III}_2Cu^{II}_3$ and $Fe^{III}_4Ni^{II}_4$ Complexes: Syntheses, Structures, and Magnetic Properties

Zhi-Guo Gu, Wei Liu, Qiao-Fang Yang, Xin-Hui Zhou, Jing-Lin Zuo,* and Xiao-Zeng You

Coordination Chemistry Institute and the State Key Laboratory of Coordination Chemistry, School of Chemistry and Chemical Engineering, Nanjing University, Nanjing 210093, People's Republic of China

Received November 29, 2006

Two tricyanometallate precursors, $(Bu_4N)[(Tp^{4Bo})Fe(CN)_3]\cdot H_2O\cdot 2MeCN$ (**1**) and $(Bu_4N)[(pzTp)Fe(CN)_3]$ (**2**) [Bu_4N^+ = tetrabutylammonium cation; Tp^{4Bo} = tris(indazolyl)hydroborate; pzTp = tetrakis(pyrazolyl)borate], with a low-spin Fe^{III} center have been synthesized and characterized. The reactions of **1** or **2** with $[Cu(Me_3tacn)(H_2O)_2](ClO_4)_2$ (Me_3tacn = *N*,*N*′,*N*″-trimethyl-1,4,7-triazacyclononane) afford two pentanuclear cyano-bridged clusters, $[(Tp^{4Bo})_2(Me_3tacn)_3Cu_3Fe_2(CN)_6](ClO_4)_4\cdot 5H_2O$ (**3**) and $[(pzTp)_2(Me_3tacn)_3Cu_3Fe_2(CN)_6](ClO_4)_4\cdot 4H_2O$ (**4**), respectively. Assembly reactions between **2** and $[Ni(phen)(CH_3OH)_4](ClO_4)_2$ (phen = 1,10-phenanthroline) or $Zn(OAc)_2\cdot 2H_2O$ afford a molecular box $[(pzTp)_4(phen)_4Ni_4Fe_4(CH_3OH)_4(CN)_{12}](ClO_4)_4\cdot 4H_2O$ (**5**) and a rectangular cluster $[(pzTp)_2Zn_2Fe_2(OAc)_2(H_2O)_2(CN)_6]$ (**6**). Their molecular structures were determined by single-crystal X-ray diffraction. In complexes **1** and **2**, the central Fe^{III} ions are coordinated by three cyanide carbon atoms and three nitrogen atoms of Tp^{4Bo-} or $pzTp^-$. Both complexes **3** and **4** show a trigonal-bipyramidal geometry, in which $[(L)Fe(CN)_3]^-$ units occupy the apical positions and are linked through cyanide to $[Cu(Me_3tacn)]^{2+}$ units situated in the equatorial plane. Complex **5** possesses a cubic arrangement of eight metal irons linked through edge-spanning cyanide bridges, while complex **6** shows $Zn_2Fe_2(CN)_4$ rectangular structure, in which Fe^{III} and Zn^{II} ions are alternately bridged by the cyanide groups. Intramolecular ferromagnetic couplings are observed for complexes **3**–**5**, and they have $S = {}^5/_2$, ${}^5/_2$, and 6 ground states and appreciable magnetic anisotropies with negative *D* values equal to –0.49, –2.39, and –0.39 cm^{-1}, respectively.

Introduction

Since the first magnetically bistable molecule, the mixed-valent dodecamanganese cluster $[Mn_{12}O_{12}(OAc)_{16}(H_2O)_4]$, was discovered in the early 1990s,[1] there is a growing interest in single-molecule magnets (SMMs).[2] SMMs exhibit slow relaxation of the magnetization below their blocking temperature derived from a large overall ground-state spin quantum number (*S*) and a significant uniaxial magnetoanisotropy (negative zero-field-splitting parameter, *D*). The combination of these factors produces a significant barrier (*U*) to thermally activated magnetization relaxation, with upper limits given by $S^2|D|$ or $(S^2 - {}^1/_4)|D|$ for integer and half-integer spins, respectively. Thus far, the majority of SMMs belong to transition metal−oxo cluster systems.[3] Cyanide, as the efficient linear bridge mediating the magnetic interaction between two metal ions, is an alternative bridging ligand for the preparation of high-spin clusters.[4,5] Moreover, it is easier to control and anticipate the topological structures and the nature (ferromagnetic vs antiferromagnetic) of the magnetic exchange interactions through the linear cyanide-bridged ligands.[6]

* To whom correspondence should be addressed. E-mail: zuojl@nju.edu.cn. Fax: +86-25-83314502.

(1) (a) Sessoli, R.; Tsai, H.-L.; Schake, A. R.; Wang, S.; Vincent, J. B.; Folting, K.; Gatteschi, D.; Christou, G.; Hendrickson, D. N. *J. Am. Chem. Soc.* **1993**, *115*, 1804. (b) Sessoli, R.; Gatteschi, D.; Caneschi, A.; Novak, M. A. *Nature* **1993**, *365*, 141.

(2) (a) Gatteschi, D.; Sessoli, R. *Angew. Chem., Int. Ed.* **2003**, *42*, 268 and references cited therein. (b) Beltran, L. M. C.; Long, J. R. *Acc. Chem. Res.* **2005**, *38*, 325 and references cited therein.

(3) For example, see: (a) Chakov, N. E.; Lee, S.-C.; Harter, A. G.; Kuhns, P. L.; Reyes, A. P.; Hill, S. O.; Dalal, N. S.; Wernsdorfer, W.; Abboud, K. A.; Christou, G. *J. Am. Chem. Soc.* **2006**, *128*, 6975. (b) Accorsi, S.; Barra, A.-L.; Caneschi, A.; Chastanet, G.; Cornia, A.; Fabretti, A. C.; Gatteschi, D.; Mortalo, C.; Olivieri, E.; Parenti, F.; Rosa, P.; Sessoli, R.; Sorace, L.; Wernsdorfer, W.; Zobbi, L. *J. Am. Chem. Soc.* **2006**, *128*, 4742. (c) Tang, J. K.; Hewitt, I.; Madhu, N. T.; Chastanet, G.; Wernsdorfer, W.; Anson, C. E.; Benelli, C.; Sessoli, R.; Powell, A. K. *Angew. Chem., Int. Ed.* **2006**, *45*, 1729. (d) Mori, F.; Nyui, T.; Ishida, T.; Nogami, T.; Choi, K.-Y.; Nojiri, H. *J. Am. Chem. Soc.* **2006**, *128*, 1440.

10.1021/ic062267q CCC: $37.00
Published on Web 03/22/2007

Chart 1

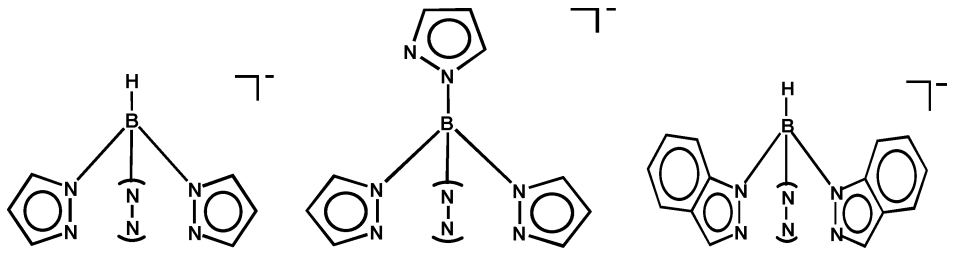

One of the most effective methods of preparing cyanometalate clusters with predictable and tunable properties is to build the polynuclear clusters step by step. In the building-block synthetic approach, it is crucial to design and prepare the building blocks, or so-called cyanometalate precursors. Recently, a new synthetic strategy for achieving cyanide-bridged molecules with higher nuclearities was reported by using multidentate-ligand-modified cyanometalates as building blocks, such as $[fac\text{-}LM(CN)_3]^{n-}$.[7−15] For example, a series of cyano-bridged molecular boxes containing $[M_4(CN)_{12}M'_4]$ ($M = Co^{III}$, Fe^{III}, Ru^{II}, Re^{II}, Re^{I}, Rh^{IV}; $M' = Co^{II}$, Ni^{II}, Mn^{II}, Rh^{III}, Co^{III}, Fe^{III}, Mo^{0}) units have been synthesized, according to the following reaction:

$$4[(L)M(CN)_3]^{x-} + 4[(L')M'(H_2O)_3]^{y+} \rightarrow [(L)_4(L')_4M_4M'_4(CN)_{12}]^{4(y-x)+} \quad (1)$$

Some of the resulting cubic clusters exhibit interesting host−gost[15] and single-molecule-magnetic[14] behaviors.

In our previous work, we employed the tris(pyrazolyl)borate tricyanometalate precursor, $(Bu_4N)[(Tp)Fe(CN)_3]$, to generate a face-centered-cubic cluster $[(Tp)_8(H_2O)_6Cu_6Fe_8(CN)_{24}]^{4+}$ exhibiting SMM-type behavior[11c] and a trigonal-bipyramidal cluster $[Tp_2(Me_3tacn)_3Cu_3Fe_2(CN)_6]^{4+}$, in which the reduced symmetry affords a significantly increased anisotropy barrier.[11d] In a continuous effort to prepare new SMMs, we have turned our attention toward designing new cyanometalate building blocks for easier control of the nuclearity and topology of the resulting clusters. As we know, the use of tris(indazolyl)hydroborate (Tp^{4Bo}) or tetrakis(pyrazolyl)borate (pzTp) instead of tris(pyrazolyl)hydroborate (Tp) in a tricyanometallate system is supposed to increase the steric effect of the capped ligand (Chart 1), which may inhibit the growth of an extended solid and promote the

(4) (a) Scuiller, A.; Mallah, T.; Verdaguer, M.; Nivorozkhin, A.; Tholence, J. L.; Veillet, P. *New J. Chem.* **1996**, *20*, 1. (b) Vostrikova, K. E.; Luneau, D.; Wernsdorfer, W.; Rey, P.; Verdaguer, M. *J. Am. Chem. Soc.* **2000**, *122*, 718. (c) Rogez, G.; Marvilliers, A.; Rivière, E.; Audière, J.-P.; Lloret, F.; Varret, F.; Goujon, A.; Mendenez, N.; Girerd, J.-J.; Mallah, T. *Angew. Chem., Int. Ed.* **2000**, *39*, 2885. (d) Berlinguette, C. P.; Vaughn, D.; Cañada-Vilalta, C.; Galán-Mascarós, J. R.; Dunbar, K. R. *Angew. Chem., Int. Ed.* **2003**, *42*, 1523. (e) Ferbinteanu, M.; Miyasaka, H.; Wernsdorfer, W.; Nakata, K.; Sugiura, K.; Yamashita, M.; Coulon, C.; Clérac, R. *J. Am. Chem. Soc.* **2005**, *127*, 3090. (f) Rebilly, J. N.; Catala, L.; Riviére, E.; Guillot, R.; Wernsdorfer, W.; Mallah, T. *Chem. Commun.* **2006**, 735.

(5) (a) Larionova, J.; Gross, M.; Pilkington, M.; Andres, H.; Stoeckli-Evans, H.; Güdel, H. U.; Decurtins, S. *Angew. Chem., Int. Ed.* **2000**, *39*, 1605. (b) Zhuang, J. Z.; Seino, H.; Mizobe, Y.; Hidai, M.; Fujishima, A.; Ohkoshi, S.; Hashimoto, K. *J. Am. Chem. Soc.* **2000**, *122*, 2952. (c) Song, Y.; Zhang, P.; Ren, X. M.; Shen, X. F.; Li, Y. Z.; You, X. Z. *J. Am. Chem. Soc.* **2005**, *127*, 3708. (d) Ruiz, E.; Rajaraman, G.; Alvarez, S.; Gillon, B.; Stride, J.; Clérac, R.; Larionova, J.; Decurtins, S. *Angew. Chem., Int. Ed.* **2005**, *44*, 2711. (e) Lim, J. H.; Yoon, J. H.; Kim, H. C.; Hong, C. S. *Angew. Chem., Int. Ed.* **2006**, *45*, 7424.

(6) (a) Entley, W. R.; Girolami, G. S. *Science* **1995**, *268*, 397. (b) Dunbar, K. R.; Heintz, R. A. *Prog. Inorg. Chem.* **1997**, *45*, 283.

(7) (a) Heinrich, J. L.; Berseth, P. A.; Long, J. R. *Chem. Commun.* **1998**, 1231. (b) Berseth, P. A.; Sokol, J. J.; Shores, M. P.; Heinrich, J. L.; Long, J. R. *J. Am. Chem. Soc.* **2000**, *122*, 9655. (c) Heinrich, J. L.; Sokol, J. J.; Hee, A. G.; Long, J. R. *J. Solid State Chem.* **2001**, *159*, 293. (d) Sokol, J. J.; Shores, M. P.; Long, J. R. *Angew. Chem., Int. Ed.* **2001**, *40*, 236. (e) Shores, M. P.; Sokol, J. J.; Long, J. R. *J. Am. Chem. Soc.* **2002**, *124*, 2279. (f) Sokol, J. J.; Hee, A. G.; Long, J. R. *J. Am. Chem. Soc.* **2002**, *124*, 7656. (g) Sokol, J. J.; Shores, M. P.; Long, J. R. *Inorg. Chem.* **2002**, *41*, 3052. (h) Yang, J. Y.; Shores, M. P.; Sokol, J. J.; Long, J. R. *Inorg. Chem.* **2003**, *42*, 1403.

(8) (a) Rebilly, J.-N.; Catala, L.; Rivière, E.; Guillot, R.; Wernsdorfer, W.; Mallah, T. *Inorg. Chem.* **2005**, *44*, 8194. (b) Rebilly, J.-N.; Catala, L.; Charron, G.; Rogez, G.; Rivière, E.; Guillot, R.; Thuéry, P.; Barra, A.-L.; Mallah, T. *Dalton Trans.* **2006**, 2818.

(9) (a) Lescouëzec, R.; Vaissermann, J.; Lloret, F.; Julve, M.; Verdaguer, M. *Inorg. Chem.* **2002**, *41*, 5943. (b) Lescouëzec, R.; Toma, L. M.; Vaissermann, J.; Verdaguer, M.; Delgado, F. S.; Ruiz-Pérez, C.; Lloret, F.; Julve, M. *Coord. Chem. Rev.* **2005**, *249*, 2691.

(10) (a) Kim, J.; Han, S.; Cho, I.; Choi, L. Y.; Heu, M.; Yoon, S.; Suh, B. J. *Inorg. Chim. Acta* **2004**, *23*, 1333. (b) Kim, J.; Han, S.; Pokhodnya, K. I.; Migliori, J. M.; Miller, J. S. *Inorg. Chem.* **2005**, *44*, 6983.

(11) (a) Wang, S.; Zuo, J.-L.; Zhou, H.-C.; Song, Y.; Gao, S.; You, X.-Z. *Eur. J. Inorg. Chem.* **2004**, 3681. (b) Wang, S.; Zuo, J. L.; Gao, S.; Song, Y.; Zhou, H. C.; Zhang, Y. Z.; You, X. Z. *J. Am. Chem. Soc.* **2004**, *126*, 8900. (c) Wang, S.; Zuo, J. L.; Zhou, H. C.; Choi, H. J.; Ke, Y.; Long, J. R.; You, X. Z. *Angew. Chem., Int. Ed.* **2004**, *43*, 5940. (d) Wang, C. F.; Zuo, J. L.; Bartlett, B. M.; Song, Y.; Long, J. R.; You, X. Z. *J. Am. Chem. Soc.* **2006**, *128*, 7162. (e) Gu, Z. G.; Yang, Q. F.; Liu, W.; Song, Y.; Li, Y. Z.; Zuo, J. L.; You, X. Z. *Inorg. Chem.* **2006**, *45*, 8895. (f) Jiang, L.; Feng, X.-L.; Lu, T.-B.; Gao, S. *Inorg. Chem.* **2006**, *45*, 5018. (g) Wen, H. R.; Wang, C. F.; Song, Y.; Gao, S.; Zuo, J. L.; You, X. Z. *Inorg. Chem.* **2006**, *45*, 8942. (h) Liu, W.; Wang, C. F.; Li, Y. Z.; Zuo, J. L.; You, X. Z. *Inorg. Chem.* **2006**, *45*, 10058.

(12) (a) Li, D.; Parkin, S.; Wang, G.; Yee, G. T.; Prosvirin, A. V.; Holmes, S. M. *Inorg. Chem.* **2005**, *44*, 4903. (b) Li, D.; Parkin, S.; Wang, G.; Yee, G. T.; Holmes, S. M. *Inorg. Chem.* **2006**, *45*, 1951. (c) Li, D.; Parkin, S.; Wang, G.; Yee, G. T.; Holmes, S. M. *Inorg. Chem.* **2006**, *45*, 2773. (d) Li, D.; Clérac, R.; Parkin, S.; Wang, G.; Yee, G. T.; Holmes, S. M. *Inorg. Chem.* **2006**, *45*, 5251.

(13) (a) Li, D.; Parkin, S.; Wang, G.; Yee, G. T.; Clérac, R.; Wernsdorfer, W.; Holmes, S. M. *J. Am. Chem. Soc.* **2006**, *128*, 4214. (b) Li, D.; Parkin, S.; Clérac, R.; Holmes, S. M. *Inorg. Chem.* **2006**, *45*, 7569.

(14) (a) Schelter, E. J.; Prosvirin, A. V.; Dunbar, K. R. *J. Am. Chem. Soc.* **2004**, *126*, 15004. (b) Schelter, E. J.; Prosvirin, A. V.; Reiff, W. M.; Dunbar, K. R. *Angew. Chem., Int. Ed.* **2004**, *43*, 4912.

(15) (a) Klausmeyer, K. K.; Rauchfuss, T. B.; Wilson, S. R. *Angew. Chem., Int. Ed.* **1998**, *37*, 1694. (b) Klausmeyer, K. K.; Wilson, S. R.; Rauchfuss, T. B. *J. Am. Chem. Soc.* **1999**, *121*, 2705. (c) Hsu, S. C. N.; Ramesh, M.; Espenson, J. H.; Rauchfuss, T. B. *Angew. Chem., Int. Ed.* **2003**, *42*, 2663. (d) Ramesh, M.; Rauchfuss, T. B. *J. Organomet. Chem.* **2004**, *689*, 1425.

construction of multinuclear clusters instead of polymers. In this paper, we report the syntheses and characterization of two stable versatile building blocks, $(Bu_4N)[(Tp^{4Bo})Fe(CN)_3]\cdot H_2O\cdot 2MeCN$ (**1**) and $(Bu_4N)[(pzTp)Fe(CN)_3]$ (**2**), and four cyano-bridged clusters based on them, $[(Tp^{4Bo})_2(Me_3tacn)_3Cu_3Fe_2(CN)_6](ClO_4)_4\cdot 5H_2O$ (**3**), $[(pzTp)_2(Me_3tacn)_3Cu_3Fe_2(CN)_6](ClO_4)_4\cdot 4H_2O$ (**4**), $[(pzTp)_4(phen)_4Ni_4Fe_4(CH_3OH)_4(CN)_{12}](ClO_4)_4\cdot 4H_2O$ (**5**), and $[(pzTp)_2Zn_2Fe_2(OAc)_2(H_2O)_2(CN)_6]$ (**6**). Their crystal structures and magnetic properties are also presented.

Experimental Section

Synthesis. All chemicals were reagent-grade and were used as received. KTp^{4Bo}, KpzTp, and $[Cu(Me_3tacn)(H_2O)_2](ClO_4)_2$ were prepared by modified literature methods.[16−18]

Caution! *The cyanides are very toxic, and perchlorate salts are potentially explosive. Thus, these starting materials should be handled in small quantities and with great caution.*

Preparation of Complex $(Bu_4N)[(Tp^{4Bo})Fe(CN)_3]\cdot H_2O\cdot 2MeCN$ (1). A mixture of KTp^{4Bo} (0.80 g, 2 mmol) in 40 mL of methanol and KCN (0.52 g, 8 mmol) in 40 mL of water was added dropwise into a solution of $FeCl_3\cdot 6H_2O$ (0.52 g, 2 mmol) in 100 mL of methanol. The color changed immediately to dark brown, and a brown powder was precipitated. After heating at 80 °C for 3 h, the resulting mixture was cooled to room temperature and filtered to remove a brown, insoluble solid. Solid $(Bu_4N)Cl$ (0.56 g, 2 mmol) was added to the filtrate and concentrated the solution to about 50 mL at 50 °C. A dark-brown powder was collected by filtration from the concentrated solution, and recrystallization from a $MeCN/Et_2O$ solution gave dark-brown block-shaped crystals of **1**. Yield: 40%. Anal. Calcd for $C_{44}H_{60}BFeN_{12}O$: C, 62.94; H, 7.20; N, 20.02. Found: C, 62.75; H, 7.31; N, 19.77. IR (KBr, cm^{-1}): 2121 (ν_{CN}).

Preparation of Complex $[Bu_4N][(pzTp)Fe(CN)_3]$ (2). A mixture of KpzTp (0.32 g, 1 mmol) and KCN (0.32 g, 5 mmol) in 30 mL of water was added into a solution of $FeCl_3\cdot 6H_2O$ (0.27 g, 1 mmol) in 30 mL of methanol. The solution color changed immediately to dark red, and a red-brown powder precipitated. After heating at 80 °C for 2 h, the solution was filtered and concentrated to 10 mL. Solid $(Bu_4N)Br$ (0.33 g, 1 mmol) was added to the solution and caused the precipitation of **2** as a yellow crystalline solid, which was filtered, washed with water, and dried under vacuum at room temperature. Yield: 65%. Yellow plate-shaped crystals suitable for X-ray analysis were obtained by recrystallization from a methanol/water solution. Anal. Calcd for $C_{31}H_{48}BFeN_{12}$: C, 56.81; H, 7.38; N, 25.64. Found: C, 56.84; H, 7.34; N, 25.67. IR (KBr, cm^{-1}): 2120 (ν_{CN}).

Preparation of Complex $[(Tp^{4Bo})_2(Me_3tacn)_3Cu_3Fe_2(CN)_6](ClO_4)_4\cdot 5H_2O$ (3). A solution of **1** (42.0 mg, 0.050 mmol) in 3 mL of acetonitrile was added to a solution of $[(Me_3tacn)Cu(H_2O)_2](ClO_4)_2$ (35.2 mg, 0.075 mmol) in 3 mL of acetonitrile, resulting in immediate formation of a brown-black solution. Diffusion of ether vapor into this solution produced dark-brown block-shaped crystals of **3**. Yield: 62%. Anal. Calcd for $C_{84}H_{130}B_2Cl_4Cu_3Fe_2N_{30}O_{20}$: C, 43.01; H, 5.59; N, 17.91. Found: C, 42.75; H, 5.74; N, 17.62. IR (KBr, cm^{-1}): 2171, 2089 (ν_{CN}).

Preparation of Complex $[(pzTp)_2(Me_3tacn)_3Cu_3Fe_2(CN)_6](ClO_4)_4\cdot 4H_2O$ (4). Complex **4** as black block-shaped crystals were synthesized from **2** and $[(Me_3tacn)Cu(H_2O)_2](ClO_4)_2$ by following the same procedure as that described for **3**. Yield: 55%. Anal. Calcd for $C_{57}H_{90}B_2Cl_4Cu_3Fe_2N_{32}O_{17.5}$: C, 35.01; H, 4.64; N, 22.21. Found: C, 34.85; H, 4.82; N, 22.06. IR (KBr, cm^{-1}): 2090, 2125, 2176 (ν_{CN}).

Preparation of Complex $[(pzTp)_4(phen)_4Ni_4Fe_4(CH_3OH)_4(CN)_{12}](ClO_4)_4\cdot 4H_2O$ (5). Solid $Ni(ClO_4)_2\cdot 6H_2O$ (19 mg, 0.05 mmol) and phen (9 mg, 0.05 mmol) were mixed in 5 mL of CH_3OH. Treatment of this mixture with **2** (33 mg, 0.05 mmol) afforded a dark-red solution, which was magnetically stirred for 10 min and then filtered. Red block-shaped crystals of **5** were obtained by diffusing ether vapor into the filtrate. Yield: 48%. Anal. Calcd for $C_{112}H_{108}B_4Cl_4Ni_4Fe_4N_{52}O_{28}$: C, 41.09; H, 3.33; N, 22.25. Found: C, 41.05; H, 3.30; N, 22.29. IR (KBr, cm^{-1}): 2169 (ν_{CN}).

Preparation of Complex $[(pzTp)_2Zn_2Fe_2(OAc)_2(H_2O)_2(CN)_6]$ (6). A mixture of methanol and water (1:1, 2 mL) was gently layered on the top of a solution of $Zn(OAc)_2\cdot 2H_2O$ (22 mg, 0.1 mmol) in water (1 mL). A solution of $[Bu_4N][(pzTp)Fe(CN)_3]$ (66 mg, 0.1 mmol) in methanol (1 mL) was added carefully as the third layer. Black crystals were obtained after 2 weeks, washed with ethanol and ether, and dried in air. Yield: 35%. Anal. Calcd for $C_{34}H_{30}B_2Fe_2N_{22}O_6Zn_2$: C, 36.90; H, 2.73; N, 27.84. Found: C, 36.93; H, 2.72; N, 27.82. IR (KBr, cm^{-1}): 2123, 2175 (ν_{CN}).

X-ray Structure Determination. The crystal structures were determined on a Siemens (Bruker) SMART CCD diffractometer using monochromated Mo Kα radiation ($\lambda = 0.710\ 73$ Å) at 293 K. Cell parameters were retrieved using *SMART* software and refined using *SAINT*[19] on all observed reflections. Data were collected using a narrow-frame method with scan widths of 0.30° in ω and an exposure time of 10 s $frame^{-1}$. The highly redundant data sets were reduced using *SAINT*[19] and corrected for Lorentz and polarization effects. Absorption corrections were applied using *SADABS*[20] supplied by Bruker. Structures were solved by direct methods using the program *SHELXL-97*.[21] The positions of the metal atoms and their first-coordination spheres were located from direct-method *E* maps; other non-hydrogen atoms were found in alternating difference Fourier syntheses and least-squares refinement cycles and, during the final cycles, refined anisotropically. One of the perchlorate ions in **3** is highly disordered, as the oxygen atoms bound to Cl3 cannot be located and fully refined. Hydrogen atoms were placed in calculated positions and refined as riding atoms with a uniform value of U_{iso}. Final crystallographic data and values of R_1 and wR are listed in Table 1.

Magnetic Susceptibility Measurements. Magnetic susceptibility measurements of polycrystalline samples were measured over the temperature range 1.8−300 K with a Quantum Design MPMS-XL7 SQUID magnetometer and using an applied magnetic field from 0.1 to 2 kOe. Field dependences of magnetization were measured using a flux magnetometer in an applied field up to 70 kOe generated by a conventional pulsed technique. Data were corrected for the diamagnetic contribution calculated from Pascal's constants.[22] The ac measurements were performed at various

(16) (a) Rheingold, A. L.; Yap, G.; Trofimenko, S. *Inorg. Chem.* **1995**, *34*, 759. (b) Janiak, C.; Temizdemir, S.; Dechert, S.; Deck, W.; Girgsdies, F.; Heinze, J.; Kolm, M. J.; Scharmann, T. G.; Zipffel, O. M. *Eur. J. Inorg. Chem.* **2000**, 1229.
(17) Trofimenko, S. *J. Am. Chem. Soc*. **1967**, *89*, 3170.
(18) Halfen, J. A.; Mahapatra, S.; Wilkinson, E. C.; Gengenbach, A. J.; Young, V. G., Jr.; Que, L., Jr.; Tolman, W. B. *J. Am. Chem. Soc*. **1996**, *118*, 763.
(19) *SAINT-Plus*, version 6.02; Bruker Analytical X-ray Systems: Madison, WI, 1999.
(20) Sheldrick, G. M. *SADABS: An empirical absorption correction program*; Bruker Analytical X-ray Systems: Madison, WI, 1996.
(21) Sheldrick, G. M. *SHELXTL-97*; Universität of Göttingen: Göttingen, Germany, 1997.
(22) Wertz, J. E.; Bolton, J. R. *Electron Spin Resonance: Elementary Theory and Practical Applications*; Chapman and Hall: New York, 1986.

Table 1. Summary of Crystallographic Data for Complexes **1**−**6**

	1	**2**	**3**	**4**	**5**	**6**
formula	$C_{44}H_{60}BFeN_{12}O$	$C_{31}H_{48}BFeN_{12}$	$C_{84}H_{130}B_2Cl_4Cu_3Fe_2N_{30}O_{20}$	$C_{57}H_{90}B_2Cl_4Cu_3Fe_2N_{32}O_{17.5}$	$C_{112}H_{108}B_4Cl_4Ni_4Fe_4N_{52}O_{28}$	$C_{34}H_{30}B_2Zn_2Fe_2N_{22}O_6$
fw	839.70	655.47	2345.92	1955.34	3273.60	1106.86
cryst syst	triclinic	orthorhombic	tetragonal	monoclinic	orthorhombic	monoclinic
space group	$P\bar{1}$	*Pbca*	$P4_2/mnm$	$P2_1/c$	*Fddd*	$P2_1/c$
a, Å	12.003(3)	14.764(4)	25.437(6)	20.375(1)	18.677(1)	11.523(5)
b, Å	13.907(3)	18.075(5)	25.437(6)	16.234(9)	30.552(4)	12.429(5)
c, Å	16.065(4)	26.875(3)	16.538(5)	31.170(1)	52.567(3)	15.784(7)
α, deg	95.43(1)	90	90	90	90	90
β, deg	109.99(7)	90	90	119.17(3)	90	95.44(2)
γ, deg	106.29(1)	90	90	90	90	90
V, Å^3	2364.2(1)	7172.24(1)	10701(5)	9002(8)	29996(3)	2250.67(6)
Z	2	8	2	2	8	4
D_{calcd}, g cm^{-3}	1.180	1.214	1.456	1.443	1.450	1.633
T/K	293(2)	293(2)	293(2)	293(2)	293(2)	293(2)
μ, mm^{-1}	0.364	0.459	1.029	1.206	1.020	1.755
θ, deg	1.92−26.00	1.52−28.27	1.79−26.00	1.70−26.00	1.54−26.00	1.78−28.23
F(000)	894	2792	4884	4024	13 376	1116
index ranges	$-14 \le h \le 13$, $-14 \le k \le 17$, $-14 \le l \le 19$	$-19 \le h \le 12$, $-24 \le k \le 14$, $-27 \le l \le 35$	$-26 \le h \le 31$, $-31 \le k \le 25$, $-20 \le l \le 20$	$-25 \le h \le 23$, $-16 \le k \le 20$, $-29 \le l \le 38$	$-23 \le h \le 22$, $-33 \le k \le 37$, $-64 \le l \le 40$	$-15 \le h \le 15$, $-16 \le k \le 16$, $-20 \le l \le 20$
no. of colld reflns	9053	8859	5639	17 620	7370	5564
no. of unique reflns	6112	5728	3727	12 800	4355	4493
no. of param	538	410	398	1081	480	308
GOF (F^2)	1.047	1.057	1.031	1.152	1.067	1.036
R1[a] [$I > 2\sigma(I)$]	0.0586	0.0440	0.0607	0.0559	0.0663	0.0294
wR2[b] [$I > 2\sigma(I)$]	0.1130	0.1115	0.1199	0.0831	0.1262	0.0798

[a] $R1 = \sum||F_o| - |F_c||/\sum F_o|$. [b] $wR2 = [\sum w(F_o^2 - F_c^2)^2/\sum w(F_o^2)]^{1/2}$.

frequencies from 1 to 1500 Hz with an ac field amplitude of 5 Oe and no dc field applied.

Other Physical Measurements. Elemental analyses for C, H, and N were performed on a Perkin-Elmer 240C analyzer. IR spectra were recorded on a Bruker Vector22 spectrophotometer with KBr pellets in the 400−4000 cm^{-1} region.

Results and Discussion

Synthesis and IR Spectroscopic Characterization. Treatment of potassium tris(indazolyl)hydroborate (KTp^{4Bo}) or potassium tetrakis(pyrazolyl)borate (KpzTp), potassium cyanide, and iron(III) chloride hexahydrate in methanol/water mixtures rapidly affords $[(Tp^{4Bo})Fe(CN)_3]^-$ and $[(pzTp)Fe(CN)_3]^-$ anions. The tetrabutylammonium salts of **1** and **2** were isolated as dark-brown and yellow crystalline solids, respectively. The preparation of the tetraethylammonium salt of **2** has been reported by Holmes et al.[12d] Complexes **1** and **2** are soluble in most organic solvents such as acetonitrile, methanol, and *N*,*N*-dimethylformamide. The IR spectra exhibit intense absorptions of ν_{CN} stretching vibrations at 2121 cm^{-1} for **1** and 2120 cm^{-1} for **2**. The cyanide stretching frequencies are comparable to those reported in poly(pyrazolyl)borate iron(III) tricyanides $[PPh_4][(Tp)Fe(CN)_3]$ (2121 cm^{-1}),[9a] $[Et_4N][(Tp^*)Fe(CN)_3]$ (2119 cm^{-1}),[12a] and $[Et_4N][(pzTp)Fe(CN)_3]$ (2120 cm^{-1}).[12d]

Slow diffusion of ether into the solution of $[Cu(Me_3tacn)(H_2O)_2](ClO_4)_2$ with **1** or **2** in acetonitrile formed dark-brown block-shaped crystals of **3** and **4** in good yield, following the reaction

$$2[fac\text{-}(L)Fe(CN)_3]^- + 3[(Me_3tacn)Cu(H_2O)_2]^{2+} \rightarrow [(L)_2(Me_3tacn)_3Cu_3Fe_2(CN)_6]^{4+} \quad (2)$$

The stretching vibrations ν_{CN} (2171 cm^{-1} for **3** and 2176 cm^{-1} for **4**) in the IR spectra are shifted to higher energies compared to those of **1** and **2**, suggesting the formation of $Fe^{III}-CN-Cu^{II}$ linkages.

In an exact parallel of eq 1, **2** reacts with $[(phen)Ni(CH_3OH)_4](ClO_4)_2$ in a methanol/ether solution to give **5**. The intense ν_{CN} stretching absorption at 2169 cm^{-1} is observed in the IR spectrum, suggesting that the bridging cyanides are present in **5**.

However, upon treatment of **2** with zinc acetate in methanol/water, a tetranuclear rectangular cluster of **6** is obtained. The ν_{CN} stretching frequencies are located at 2123 and 2175 cm^{-1} for **6**, which are consistent with the presence of terminal and bridging cyanide ligands.

Structural Description. The crystal structures of complexes **1**−**6** were determined by single-crystal X-ray analyses. In complexes **1** and **2**, the tricyanide anions display *fac* stereochemistry and the central Fe^{III} ions are six-coordinated with three cyanide carbon atoms and three nitrogen atoms of Tp^{4Bo-} or $pzTp^-$, as shown in Figures 1 and 2. Relevant bond distances and angles are listed in Tables 2 and 3. Good agreement is observed between the $Fe^{III}-C$(cyano) bond lengths [**1**, 1.893(3)−1.928(3) Å; **2**, 1.915(2)−1.921(2) Å] and those in low-spin tricyano iron(III) complexes $[Ph_4P][(Tp)Fe(CN)_3]$ [1.910(6)−1.929(7) Å] and $[Et_4N][(Tp^*)Fe(CN)_3]$ [1.899(2)−1.908(2) Å].[9a,12a] In **1**, the neighboring $[(Tp^{4Bo})Fe(CN)_3]^-$ anions weakly interact through face-to-face $\pi-\pi$ stacking interactions of the ring−centroid (in the range of about 3.571−3.673 Å), which leads to a one-dimensional (1D) zigzag chain along the *b* axis. The 1D chains are further linked through the hydrogen bonds between crystallized water molecules and cyano ligands (2.869 Å for

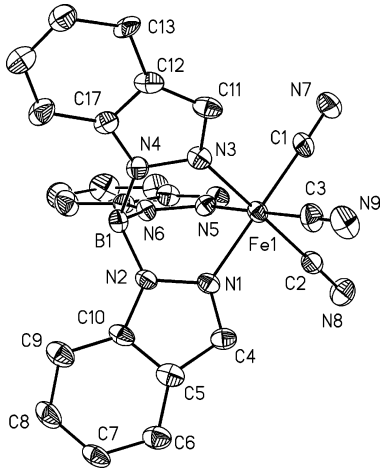

Figure 1. Perspective drawing of the anion of complex **1** showing the atom numbering scheme. Thermal ellipsoids are drawn at the 30% probability level. H atoms are omitted for clarity.

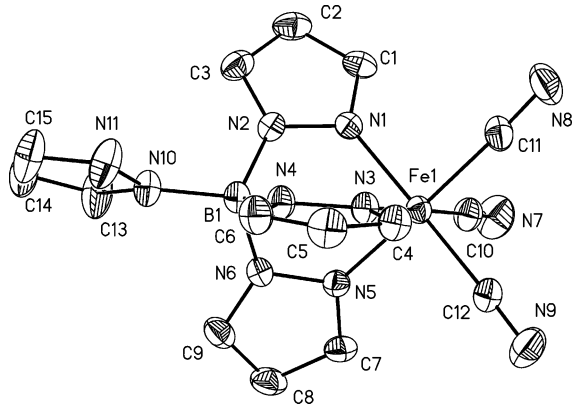

Figure 2. Perspective drawing of the anion of complex **2** showing the atom numbering scheme. Thermal ellipsoids are drawn at the 30% probability level. H atoms are omitted for clarity.

Table 2. Selected Bond Lengths (Å) and Angles (deg) for **1**

Fe1−C1	1.910(3)	Fe1−C2	1.928(3)
Fe1−C3	1.893(3)	Fe1−N1	1.984(2)
Fe1−N3	1.979(2)	Fe1−N5	1.972(2)
O1···N7	3.014(4)	O1···N9	2.869(4)
C3−Fe1−C1	88.81(1)	C3−Fe1−C2	88.15(1)
C2−Fe1−C1	87.81(1)	N1−Fe1−N3	91.50(1)
N5−Fe1−N3	88.47(9)	N1−Fe1−N5	88.36(1)
N7−C1−Fe1	178.5(3)	N9−C3−Fe1	177.9(3)
N8−C2−Fe1	179.1(3)	O1−H1A−N9	147.3(2)
O1−H1B−N7	126.5(2)		

Table 3. Selected Bond Lengths (Å) and Angles (deg) for **2**

Fe1−C1	1.922(2)	Fe1−C2	1.915(2)
Fe1−C3	1.921(2)	Fe1−N4	1.966(2)
Fe1−N6	1.984(2)	Fe1−N8	1.979(2)
C2−Fe1−C3	89.30(9)	C2−Fe1−C1	87.43(9)
C3−Fe1−C1	88.92(9)	N4−Fe1−N6	87.17(6)
N4−Fe1−N8	88.86(6)	N1−C1−Fe1	179.6(2)
N8−Fe1−N6	87.40(6)	N3−C3−Fe1	175.8(2)
N2−C2−Fe1	176.9(2)		

O1···N9 and 3.014 Å for O1···N7), forming a layered structure (Figure S1 in the Supporting Information). The shortest intermolecular Fe−Fe separations are 8.711 and 7.848 Å for **1** and **2**, respectively.

Table 4. Selected Bond Lengths (Å) and Angles (deg) for **3**

Fe1−C15	1.871(4)	Fe1−C21	1.907(6)
Fe1−N1	1.948(4)	Fe1−N3	1.941(5)
Cu1−N5	1.940(4)	Cu1−N6	2.085(5)
Cu1−N7	2.044(3)	Cu2−N8	2.030(5)
Cu2−N9	2.107(5)	Cu2−N10	2.016(4)
N5−C15−Fe1	177.1(4)	N8−C21−Fe1	169.5(6)
C15−Fe1−C21	88.37(2)	C15−Fe1−C15A	85.8(3)
N1−Fe1−N1A	84.9(2)	N1−Fe1−N3	89.05(1)
C15−N5−Cu1	168.0(3)	N5−Cu1−N5A	87.4(2)
N5−Cu1−N7	175.17(2)	N5A−Cu1−N7	94.49(1)
N5−Cu1−N6	98.49(1)	N6−Cu1−N7	85.64(1)
N7−Cu1−N7A	83.29(2)	C21−N8−Cu2	177.0(5)
N8−Cu2−N8A	83.4(3)	N8−Cu2−N10	156.46(1)
N8A−Cu2−N10	91.40(2)	N8−Cu2−N9	117.32(1)
N9−Cu2−N10	85.46(1)	N10−Cu2−N10A	101.83(2)

Table 5. Selected Bond Lengths (Å) and Angles (deg) for **4**

Fe1−C13	1.935(3)	Fe1−C14	1.915(3)
Fe1−C15	1.930(3)	Fe2−C28	1.942(3)
Fe2−C29	1.913(3)	Fe2−C30	1.918(3)
Fe1−N1	1.942(3)	Fe1−N3	1.959(3)
Fe1−N5	1.962(2)	Fe2−N15	1.967(3)
Fe2−N17	1.948(3)	Fe2−N19	1.988(3)
Cu1−N9	1.978(3)	Cu1−N12	1.961(3)
Cu1−N23	2.031(2)	Cu1−N24	2.191(2)
Cu1−N25	2.060(3)	Cu2−N11	2.001(3)
Cu2−N14	1.993(3)	Cu2−N29	2.219(3)
Cu2−N30	2.084(3)	Cu2−N31	2.050(2)
Cu3−N10	2.000(3)	Cu3−N13	1.951(2)
Cu3−N26	2.061(3)	Cu3−N27	2.207(3)
Cu3−N28	2.082(2)		
N9−C13−Fe1	178.0(2)	N10−C14−Fe1	175.0(2)
N11−C15−Fe1	178.8(3)	N12−C30−Fe2	178.6(3)
N13−C28−Fe2	177.8(3)	N14−C29−Fe2	175.3(3)
C14−Fe1−C15	89.14(1)	C15−Fe1−C13	88.61(1)
C15−Fe1−C13	88.73(1)	C29−Fe2−C30	89.75(1)
C29−Fe2−C28	89.53(1)	C28−Fe2−C30	90.06(1)
C13−N9−Cu1	167.6(4)	C30−N12−Cu1	172.8(2)
C15−N11−Cu2	170.6(2)	C29−N14−Cu2	170.9(2)
C14−N10−Cu3	168.5(9)	C28−N13−Cu3	170.8(9)
N9−Cu1−N12	88.35(1)	N11−Cu2−N14	86.19(1)
N10−Cu3−N13	87.33(1)		

Table 6. Selected Bond Lengths (Å) and Angles (deg) for **5**

Fe1−C13	1.935(5)	Fe1−C14	1.924(6)
Fe1−C15	1.948(6)	Fe1−N1	1.984(4)
Fe1−N3	1.939(4)	Fe1−N5	1.971(4)
Ni1−N9	2.039(4)	Ni1−N10	2.038(4)
Ni1−N11	2.022(4)	Ni1−N12	2.085(4)
Ni1−N13	2.095(4)	Ni1−O1	2.099(3)
C13−Fe1−C14	87.22(1)	C13−Fe1−C15	89.28(1)
C14−Fe1−C15	88.0(2)	N1−Fe1−N3	90.09(1)
N1−Fe1−N5	87.08(1)	N3−Fe1−N5	89.14(7)
N9−C13−Fe1	178.8(4)	N10−C14−Fe1	177.7(5)
N11−C15−Fe1	177.2(5)	C13−N9−Ni1	170.5(4)
C14−N10−Ni1	171.4(4)	C15−N11−Ni1	172.8(4)
N9−Ni1−N10	93.36(1)	N9−Ni1−N11	90.42(1)
N10−Ni1−N11	91.97(1)	O1−Ni1−N9	90.49(1)
O1−Ni1−N10	90.78(1)	O1−Ni1−N11	177.05(1)
O1−Ni1−N12	88.27(1)	O1−Ni1−N13	89.40(1)

The crystal structures for **3** and **4** are very similar to our recently reported complex $[Tp_2(Me_3tacn)_3Cu_3Fe_2(CN)_6](ClO_4)_4 \cdot 2H_2O$[11d] and are depicted in Figure 3 and Figure S2 in the Supporting Information. Complex **3** crystallizes in the tetragonal $P4_2/mnm$ space group, while complex **4** crystallizes in the monoclinic $P2_1/c$ space group. In complex **3**, the Me_3-tacn ligand coordinated to the Cu2 ion is disordered and occupies two positions equally with a ratio of 0.5:0.5.

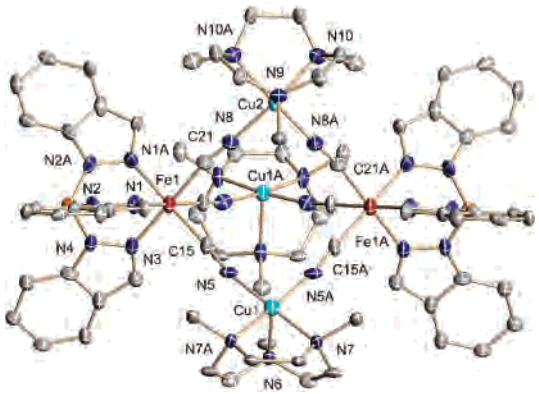

Figure 3. Perspective drawing of the trigonal-bipyramidal cluster of $[(Tp^{4Bo})_2(Me_3tacn)_3Cu_3Fe_2(CN)_6]^{4+}$ in **3** showing the atom numbering scheme. Thermal ellipsoids are drawn at the 30% probability level. H atoms are omitted for clarity.

Table 7. Selected Bond Lengths (Å) and Angles (deg) for **6**

Fe1−C1	1.925(2)	Fe1−C2	1.920(2)
Fe1−C3	1.916(2)	Fe1−N4	1.970(2)
Fe1−N6	1.954(2)	Fe1−N8	1.966(2)
Zn1−O1	1.966(2)	Zn1−O2	1.924(2)
Zn1−N2	1.973(2)	Zn1−N3	1.995(2)
C2−Fe1−C3	86.47(9)	C2−Fe1−C1	87.79(9)
C3−Fe1−C1	89.27(9)	N8−Fe1−N6	89.14(7)
N4−Fe1−N8	87.96(7)	N4−Fe1−N6	88.65(7)
N1−C1−Fe1	175.0(2)	N2−C2−Fe1	177.2(2)
N3−C3−Fe1	179.4(2)	O1−Zn1−O2	102.97(8)
O2−Zn1−N2	130.56(8)	O1−Zn1−N2	109.48(9)
O2−Zn1−N3	105.82(8)	O1−Zn1−N3	101.88(8)
N2−Zn1−N3	102.82(8)	N2−C2−Zn1	170.7(2)
N3−C3−Fe1	172.4(2)		

Relevant bond distances and angles for **3** and **4** are listed in Tables 4 and 5, respectively. Both clusters have a trigonal-bipyramidal geometry, in which three square-pyramidal $[Cu(Me_3tacn)]^{2+}$ units are situated in the equatorial plane that are bridged through cyanide to two $[(Tp^{4Bo})Fe(CN)_3]^-$ or $[(pzTp)Fe(CN)_3]^-$ units occupying the apical positions. In both complexes, each Fe^{III} ion possesses a distorted octahedral coordination environment. The Cu^{II} ions are coordinated to a Me_3tacn ligand as well as two nitrogen atoms of two cyanide bridges, forming a square-pyramidal coordination conformation. The basal positions of the square pyramid are occupied by two cyanide nitrogen atoms and two Me_3tacn nitrogen atoms with bond lengths distributed within the range 1.940(4)−2.044(3) Å for **3** and 1.951(2)−2.082(2) Å for **4**. The apical position is occupied by the remaining nitrogen atom of the Me_3tacn ligand with much longer bond lengths [2.085(5)−2.107(5) Å for **3** and 2.191(2)−2.219(3) Å for **4**]. All of the cyanide bridges in the cluster deviate somewhat from linearity, as is reflected in the Fe−C−N and Cu−N−C angles, which range from 168.0(3) to 177.1(4)° for **3** and from 167.6(4) to 178.8(3)° for **4**. The shortest intramolecular $Fe^{III}\cdots Cu^{II}$, $Fe^{III}\cdots Fe^{III}$, and $Cu^{II}\cdots Cu^{II}$ separations are 4.991, 6.390, and 6.632 Å for **3** and 5.008, 6.294, and 6.437 Å for **4**, whereas the shortest intermolecular $Fe^{III}\cdots Cu^{II}$, $Fe^{III}\cdots Fe^{III}$, and $Cu^{II}\cdots Cu^{II}$ distances are 10.713, 11.700, and 8.650 Å in complex **3** and 8.354, 9.948, and 8.680 Å in complex **4**, respectively. In complex **3**, there is a weak T-shaped C−H$\cdots\pi$ contact (2.952 Å) between the Tp^{4Bo} ligands that

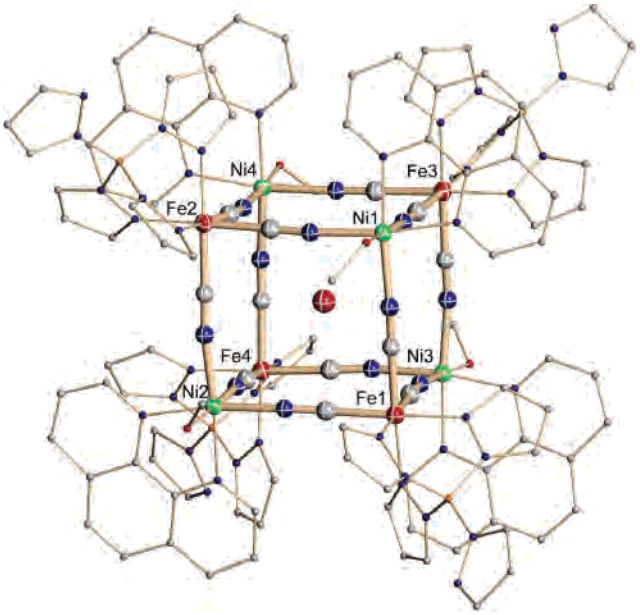

Figure 4. Perspective drawing of the cubic cluster of $[(pzTp)_4(Phen)_4Ni_4Fe_4(CH_3OH)_4(CN)_{12}]^{4+}$ in **5**. Thermal ellipsoids of the central core are drawn at the 30% probability level. The remaining atoms are depicted in stick mode, and H atoms are omitted for clarity. Color coding: Fe, dark red; Ni, green; B, orange; C, gray; N, blue; O, light red.

results in the formation of a two-dimensional (2D) network, as shown in Figure S3 in the Supporting Information. In complex **4**, there is no significant intermolecular interaction because the nearest pyridyl rings from adjacent molecules are not overlapped.

Complex **5** crystallizes in the orthorhombic *Fddd* space group; it contains Fe^{III} and Ni^{II} centers, which reside in alternate corners of a slightly distorted box and are bridged by 12 cyanide ligands (Figure 4). Very recently, Holmes et al. have reported some similar cyano-bridged $Fe^{III}_4Ni^{II}_4$ cubes.[13] However, the motif for **5** represents the fundamental cage unit in the Prussian blue structure type,[23] isolated by virtue of the outer capping ligand pzTp on each Fe^{III} center and 1,10-phenanthroline on each Ni^{II} center. The octanuclear $[(pzTp)_4(phen)_4Ni_4Fe_4(CH_3OH)_4(CN)_{12}]^{4+}$ in **5** defines a central cavity, and a water molecule occupies the vacancy volume of the cubic cage. As we know, it is very common that alkali-metal cations occupy such positions.[15] However, to the best of our knowledge, we cannot find other examples of the presence of water within the analogous cages of $M_4(CN)_{12}M'_4$ complexes in the literature. The boxlike cages are highly symmetrical, as reflected in the bond angles of Fe−C−N [177.2(5)−178.8(4)°], Cu−N−C [170.5(4)−172.7(5)°], C−Fe−C [87.2(2)−89.2(8)°], and N−Ni−N [87.5(3)−91.9(7)°]. The bridging cyanide Fe−C and Ni−N bond distances range from 1.924(6) to 1.948(6) Å and from 2.022(4) to 2.039(4) Å. The corresponding average edge (Fe^{III}−Ni^{II}), face (Fe^{III}−Fe^{III}), and body-diagonal (Fe^{III}−Ni^{II}) distances are ca. 5.09(2), 7.27(9), and 8.81(5) Å, respectively. In **5**, there are weak intermolecular $\pi-\pi$ stacking interactions

(23) Buser, H. J.; Schwarzenbach, D.; Petter, W.; Ludi, A. *Inorg. Chem.* **1977**, *16*, 2704.
(24) Kahn, O. *Molecular Magnetism*; VCH, Weinheim, Germany, 1993; p 26.

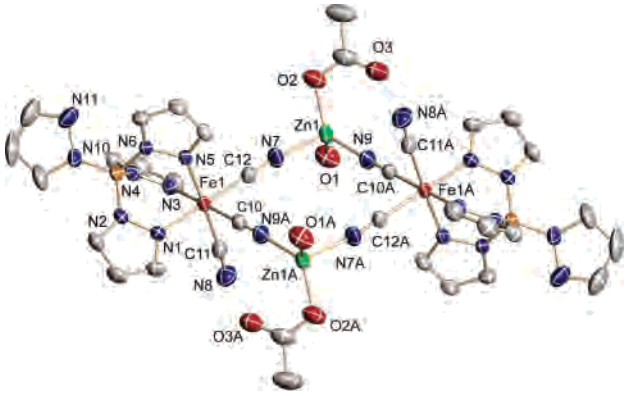

Figure 5. Perspective drawing of complex **6** showing the atom numbering scheme. Thermal ellipsoids are drawn at the 30% probability level. H atoms are omitted for clarity.

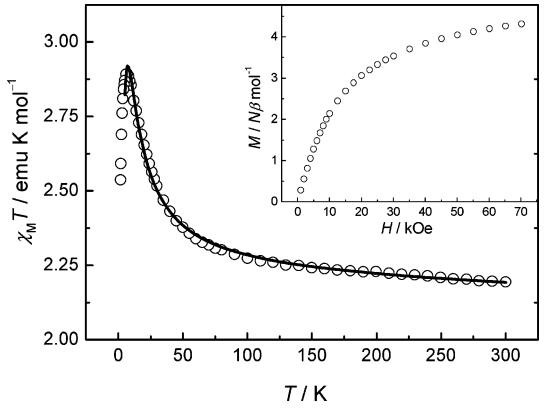

Figure 6. Temperature dependence of the $\chi_M T$ product for **3** at 2 kOe. Solid lines represent the best fit of the data. The inset shows the magnetization versus the applied magnetic field at 1.8 K.

between two adjacent phen molecules coordinated to Ni^{II}, resulting in a 2D sheet structure with a ring−centroid distance of 3.518 Å (Figure S4 in the Supporting Information).

Complex **6** crystallizes in the monoclinic $P2_1/c$ space group; the rectangular cluster is composed of the alternately four-coordinated Zn^{II} ions and $[(pzTp)Fe(CN)_3]^-$ anions (Figure 5). The $[(pzTp)Fe(CN)_3]^-$ acts as a bidentate ligand to bridge Zn^{II} ions through two of its three cyanide groups in the cis positions. The bridging cyano ligands coordinate to the Zn^{II} ion [Zn−N = 1.973(2) and 1.995(2) Å] in a bent fashion with Zn−N≡C bond angles of 170.7(2)° and 172.4(2)°, respectively. The remaining coordination positions of each Zn^{II} ion are occupied by two oxygen atoms of one acetic anion and one water molecule with Zn−O bond distances of 1.924(2) and 1.966(2) Å. Each discrete $[(pzTp)_2Zn_2Fe_2(OAc)_2(H_2O)_2(CN)_6]$ molecule is linked to four adjacent Zn_2Fe_2 molecules through hydrogen-bonding interactions to generate a 2D network structure (Figure S5 in the Supporting Information).

Magnetic Properties. Magnetic measurements were performed on polycrystalline samples of complexes **1**, **3**, **4**, and **5**. For complex **1**, at room temperature, the $\chi_M T$ value is 0.66 emu K mol^{-1} (Figure S6 in the Supporting Information), which is much higher than the spin-only value of 0.375 emu K mol^{-1} ($g = 2.0$) expected for low-spin distorted octahedral Fe^{III} ions ($S = {}^1/_2$). This indicates that there exists significant spin−orbit coupling of the $^2T_{2g}$ ground term for Fe^{III} ions in **1**.[25] Between 300 and 20 K, the $\chi_M T$ values exhibit a quasi-linear dependence with T from 0.66 to 0.46 emu K mol^{-1} and then decrease smoothly below ca. 10 K, reaching a minimum value of 0.33 emu K mol^{-1} at 1.8 K.

The susceptibility variations in different temperatures of **3** were measured in 1.8−300 K (Figure 6). At 300 K, its $\chi_M T$ value is 2.19 emu K mol^{-1}, which is slightly higher than the spin-only value of 1.875 emu K mol^{-1} ($g = 2.0$) expected for two low-spin Fe^{III} ($S = {}^1/_2$) and three Cu^{II} ($S = {}^1/_2$) ions in the absence of any exchange coupling. As the temperature decreases, $\chi_M T$ gradually increases and reaches 2.38 emu K mol^{-1} at 50 K, and then it abruptly increases, reaching a maximum of 2.89 emu K mol^{-1} at approximately 7 K, suggesting ferromagnetic coupling resulting from the orthogonal spin orbitals of the Fe^{III} (t_{2g}) and square-pyramidal Cu^{II} (b_{1g}) centers. This magnetic nature could be further supported by the apparently unsaturated magnetization value of 4.31 $N\beta$ mol^{-1} under a 7 kOe magnetic field at 1.8 K, confirming an $S = {}^5/_2$ ground state for the cluster (inset in Figure 6). Below 6 K, $\chi_M T$ sharply drops to 2.54 emu K mol^{-1} at 1.8 K, which is attributed to the presence of zero-field splitting and/or intermolecular interactions.

The interaction parameters between Fe^{III} and Cu^{II} in **3** were determined from least-squares fitting of the theoretical expression given in eq 3, deduced from the spin Hamiltonian:

$$\hat{H} = -2J_{FeCu}(\hat{S}_{Fe1} + \hat{S}_{Fe2})(\hat{S}_{Cu1} + \hat{S}_{Cu2} + \hat{S}_{Cu3}) - 2J_{CuCu}(\hat{S}_{Cu1}\hat{S}_{Cu2} + \hat{S}_{Cu2}\hat{S}_{Cu3} + \hat{S}_{Cu3}\hat{S}_{Cu1}) - 2J_{FeFe}\hat{S}_{Fe1}\hat{S}_{Fe2}$$

$$\chi_M = \frac{Ng^2\beta^2}{4kT} \frac{2e^{(5J_{FeCu}-3J_{CuCu}-2J_{FeFe})/kT} + 10e^{(5J_{FeCu}-2J_{FeFe})/kT} + 2e^{(3J_{FeCu}-3J_{CuCu})/kT} + 20e^{(6J_{FeCu}-3J_{CuCu})/kT} + 1 + 10e^{3J_{FeCu}/kT} + 35e^{8J_{FeCu}/kT}}{2e^{(5J_{FeCu}-3J_{CuCu}-2J_{FeFe})/kT} + 2e^{(5J_{FeCu}-2J_{FeFe})/kT} + 2e^{(3J_{FeCu}-3J_{CuCu})/kT} + 4e^{(6J_{FeCu}-3J_{CuCu})/kT} + 1 + 2e^{3J_{FeCu}/kT} + 3e^{8J_{FeCu}/kT}} \quad (3)$$

To take into account the decrease of $\chi_M T$ below 7 K, the intermolecular interactions (zJ') within the mean-field approximation have been considered.[24] Assuming $J_{CuCu} = J_{FeFe} = 0$, the best-fit results between 4 and 300 K with a TIP correction were obtained: $g = 2.28$, $J_{FeCu} = 3.45$ cm^{-1}, $zJ' = -0.44$ cm^{-1}, and TIP $= 2.3 \times 10^{-4}$ emu mol^{-1} ($R = 2.3 \times 10^{-4}$).

The magnetization variation for **3** at different magnetic fields was recorded between 1.8 and 10 K (Figure 7). The nonsuperposition of the isofield lines indicates the presence of significant zero-field splitting. With the spin ground state $S = {}^5/_2$, fits of the magnetization data using ANISOFIT[7e] for $T \leq 10$ K and $H \geq 10$ kOe afford $D = -0.49$ cm^{-1} and $E = 9.4 \times 10^{-2}$ cm^{-1}.

(25) (a) Patra, A. K.; Ray, M.; Mukherjee, R. *Inorg. Chem.* **2000**, *39*, 652. (b) Martin, L. L.; Martin, R. L.; Murray, K. S.; Sargeson, A. M. *Inorg. Chem.* **1990**, *29*, 1387. (c) Toma, L. M.; Lescouëzec, R.; Toma, L. D.; Lloret, F.; Julve, M.; Vaissermann, J.; Andruh, M. *J. Chem. Soc., Dalton Trans.* **2002**, 3171.

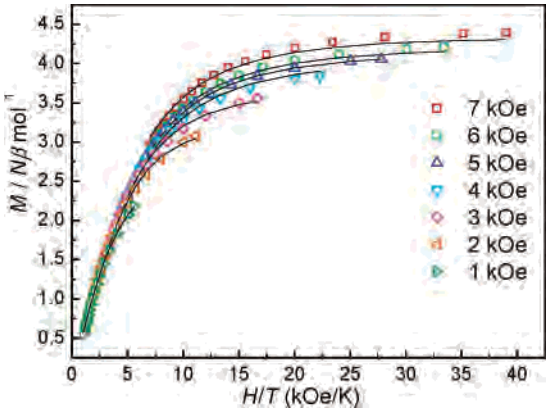

Figure 7. Plot of magnetization vs *H*/*T* for **3** between 1.8 and 10 K. Solid lines represent the best fits to the data.

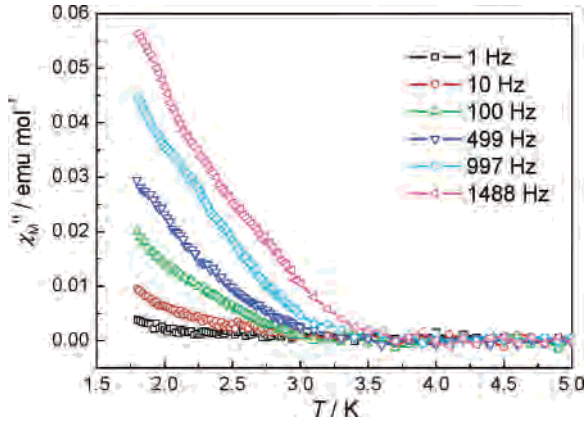

Figure 8. Out-of-phase component of the ac susceptibility at different frequencies for **3**.

The ac susceptibility measurements were performed on a sample of **3** in a 5 Oe ac field oscillating at 1−1488 Hz with a zero applied dc field (Figure 8). Although the χ_M' vs *T* plot shows no obvious frequency dependence above 1.8 K (see Figure S5 in the Supporting Information), the out-of-phase magnetic susceptibility (χ_M'') signals show nonzero and a rather smaller frequency dependence, indicating that a slow relaxation of the magnetization may occur at lower temperature. Initially, these types of small χ_M'' signals, together with an apparent simple frequency dependence, were attributed to an undefined magnetic species, yet they have been taken as evidence for the presence of slow magnetization relaxation in some recently reported complexes, $[(pzTp)Fe^{III}(CN)_3]_4[Ni^{II}L]_4[OTf]_4$ [L = 2,2,2-tris(pyrazolyl)ethanol],[13a] $[Ni(hmp)(ROH)Cl]_4$ [hmp = 2-(hydroxymethyl)pyridine],[26a] $[Mn_{12}O_2(OMe)_2(thme)_4(OAc)_{10}(H_2O)_4]$ [H_3thme = 1,1,1-tris(hydroxymethyl)-methane],[26b] $[Mn_2(5\text{-MeOsaltmen})_2(DCNNQI)_2]$ (DCNNQI = *N*,*N*′-dicyano-1,4-naphthoquinonediiminate).[26c] Unfortunately, there is no maximum for the χ_M'' signals down to 1.8 K. Further magnetic measurements at lower temperature should be performed to confirm the SMM properties.

(26) (a) Yang, E.-C.; Wernsdorfer, W.; Zakharov, L. N.; Karaki, Y.; Yamaguchi, A.; Isidro, R. M.; Lu, G.-D.; Wilson, S. A.; Rheingold, A. L.; Ishimoto, H.; Hendrickson, D. N. *Inorg. Chem.* **2006**, *45*, 529. (b) Li, Y.; Wernsdorfer, W.; Clerac, R.; Hewitt, I. J.; Anson, C. E.; Powell, A. K. *Inorg. Chem.* **2006**, *45*, 2376. (c) Kachi-Terajima, C.; Miyasaka, H.; Sugiura, K.-i.; Clerac, R.; Nojiri, H. *Inorg. Chem.* **2006**, *45*, 4381.

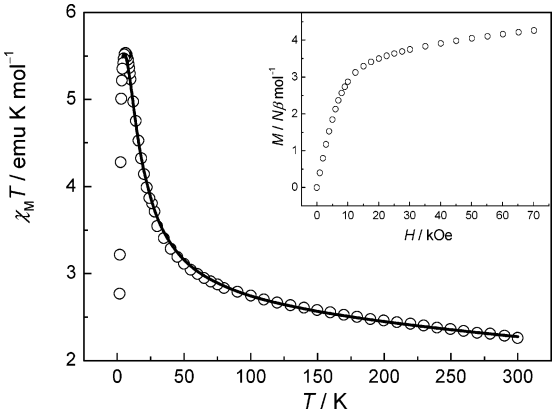

Figure 9. Temperature dependence of the $\chi_M T$ product for **4** at 2 kOe. Solid lines represent the best fits to the data. The inset shows the magnetization versus the applied magnetic field at 1.8 K.

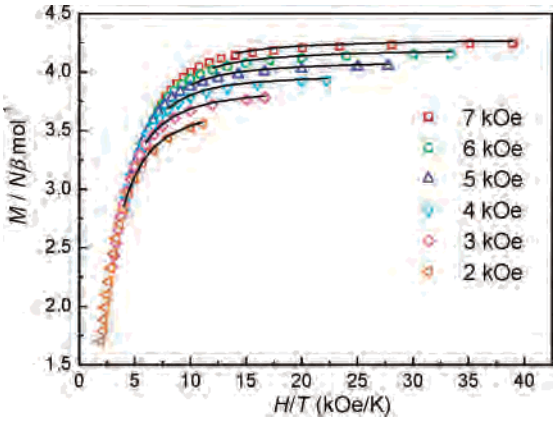

Figure 10. Plot of magnetization vs *H*/*T* for **4** between 1.8 and 10 K. Solid lines represent the best fits to the data.

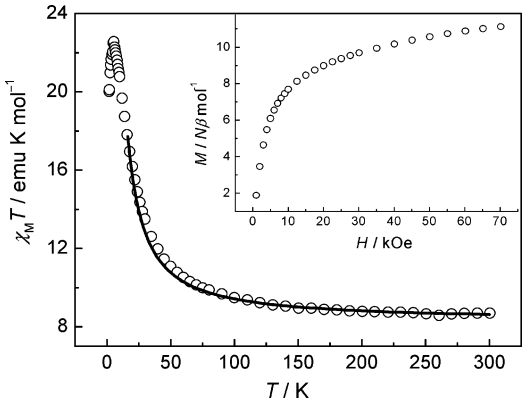

Figure 11. Temperature dependence of the $\chi_M T$ product for **5** at 0.1 kOe. Solid lines represent the best fits to the data. The inset shows the magnetization versus the applied magnetic field at 1.8 K.

The temperature dependence of susceptibility for complex **4** is displayed in Figure 9. Upon lowering of the temperature, the $\chi_M T$ value increases continuously from the room-temperature value of 2.27 emu K mol^{-1} and then reaches a maximum of 5.54 emu K mol^{-1} at 6.5 K, indicating ferromagnetic interaction between Fe^{III} and Cu^{II}, which can be further supported by the apparently unsaturated magnetization value of 4.26 $N\beta$ mol^{-1} under a 70 kOe magnetic field (inset in Figure 9). Below 6.5 K, $\chi_M T$ drops down sharply, reaching 1.54 emu K mol^{-1} at 1.8 K. The $\chi_M T$ data are simulated with the same Hamiltonian as that of **3**, and

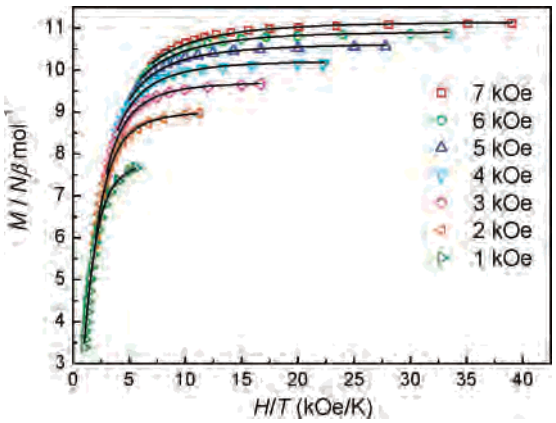

Figure 12. Plot of magnetization vs H/T for **5** between 1.8 and 10 K. Solid lines represent the best fits to the data.

the fitting results between 6.5 and 300 K are $g = 2.28$, $J_{FeCu} = 7.92$ cm^{-1}, $zJ' = -0.030$ cm^{-1}, and TIP $= 1.18 \times 10^{-3}$ emu mol^{-1} ($R = 2.2 \times 10^{-3}$). In the M vs H/T plot, the nonsuperposition of the lines in different magnetic fields is observed (Figure 10), suggesting the existence of zero-field splitting. With the spin ground state $S = {}^5/_2$, fits of the magnetization data using ANISOFIT[7e] for $T \leq 5$ K and $H \geq 20$ kOe afforded $D = -2.39$ cm^{-1} and $E = 0.36$ cm^{-1}. The ac susceptibility studies carried out in the 1.8−10 K range in a 5Oe oscillating field at frequencies up to 1500 Hz for **3** showed no evidence for magnetic ordering or slow paramagnetic relaxation.

We note that the axial anisotropy of **3** ($D = -0.49$ cm^{-1}; crystallized in the $P4_2/mnm$ space group) is much smaller than those of the clusters **4** ($D = -2.39$ cm^{-1}; crystallized in the $P2_1/c$ space group) and $[Tp_2(Me_3tacn)_3Cu_3Fe_2(CN)_6]^{4+}$ ($D = -5.7$ cm^{-1}; also crystallized in the $P2_1/c$ space group),[11d] although they show nearly the same topology and spin state. These results show the significant impact that symmetry structural distortion of the cluster core can have on magnetic anisotropy, which may lead to enhancement of the overall anisotropy. Furthermore, the obvious crystallographic disorder and intermolecular C−H···π stacking interactions in **3** may also account for the significantly decreased axial anisotropy.

The temperature variation of susceptibility for complex **5** is displayed in Figure 11. Upon lowering of the temperature, the $\chi_M T$ value increases continuously from the room-temperature value of 8.29 emu K mol^{-1}, followed by a rapid increase below 45 K with a maximum of 22.56 emu K mol^{-1} at 5.5 K, indicating ferromagnetic interaction between Fe^{III} and Ni^{II}. This can be further supported by the apparently unsaturated magnetization value of 11.11 $N\beta$ mol^{-1} under a 70 kOe magnetic field (inset in Figure 11). Below 5.5 K, $\chi_M T$ drops down sharply, reaching 20.01 emu K mol^{-1} at 1.8 K, which could be attributed to the zero-field splitting and/or weak antiferromagnetic interactions between the clusters. According to the structures, the exchange Hamiltonian of **5** can be described as

$$\hat{H} = -2J_{FeNi}[\hat{S}_{Ni1}(\hat{S}_{Fe1} + \hat{S}_{Fe2} + \hat{S}_{Fe3}) + \hat{S}_{Ni2}(\hat{S}_{Fe1} + \hat{S}_{Fe2} + \hat{S}_{Fe4}) + \hat{S}_{Ni3}(\hat{S}_{Fe1} + \hat{S}_{Fe3} + \hat{S}_{Fe4}) + \hat{S}_{Ni4}(\hat{S}_{Fe2} + \hat{S}_{Fe3} + \hat{S}_{Fe4})]$$

The best-fit results by using the MAGPACK program (MAGPACK)[27] were obtained from 300 to 6 K: $g = 2.45$ and $J_{FeNi} = 6.0$ cm^{-1}. The magnetization variation for **5** at different magnetic fields was recorded between 1.8 and 10 K. As shown in Figure 12, the nonsuperposition of the isofield lines indicates the presence of significant zero-field splitting. With the spin ground state $S = 6$, least-squares fitting of the M vs H/T data (ANISOFIT)[7e] affords $D = -0.39$ cm^{-1} and $E = 0.11$ cm^{-1}, suggesting that the maximum energy barrier for **5** is $U = S^2|D| = 14.0$ cm^{-1}.

To investigate the dynamic nature of complex **5**, the ac susceptibility was measured in the frequency range of 1−1488 Hz at 1.8−10 K with zero applied dc field (Figures S8 and S9 in the Supporting Information), which shows a similar trend like the ever-reported octanuclear cubic $Fe^{III}_4Ni^{II}_4$ complexes.[13] The χ_M' vs T plot shows no obvious frequency dependence above 1.8 K, while the small frequency-dependent signals in out-of-phase susceptibilities (χ_M'') observed below 5 K suggest that complex **5** exhibits slow magnetization relaxation.

In summary, two new C_3 symmetric facially tricyanide-containing building blocks **1** and **2** were successfully synthesized. Using **1** and **2** as building blocks, two trigonal-bipyramidal $Fe^{III}_2Cu^{II}_3$ (**3** and **4**), a cubic $Fe^{III}_4Ni^{II}_4$ molecule box (**5**), and a tetranuclear rectangular $Fe^{III}_2Zn^{II}_2$ (**6**) were synthesized and structurally characterized. Magnetic studies for complexes **3**−**5** show ferromagnetic coupling, giving $S = {}^5/_2$, ${}^5/_2$, and 6 ground states and appreciable magnetic anisotropy with negative D values equal to −0.49, −2.39, and −0.39 cm^{-1}, respectively. The ac magnetic susceptibilities of **3** and **5** exhibit the characteristics of slow magnetization relaxation. In the literature, the cyano-bridged SMMs are still less studied. The present results suggest that mononuclear compounds **1** and **2** are possible versatile building blocks for assembling new cyanide-bridged heterometallic high-spin clusters with interesting magnetic properties.

Acknowledgment. This work was supported by the National Natural Science Foundation of China (Grants 20531040 and 90501002), the Major State Basic Research Development Program (Grant 2006CB806104), the Program for New Century Excellent Talents in University of China (Grant NCET-04-0469), and the Natural Science Foundation of Jiangsu Province (Grant BK2006512).

Supporting Information Available: X-ray crystallographic files in CIF format for **1**−**6**, structural figures, and additional magnetic data. This material is available free of charge via the Internet at http://pubs.acs.org.

IC062267Q

(27) (a) Borras-Almenar, J. J.; Clemente-Juan, J. M.; Coronado, E.; Tsukerblat, B. S. *J. Comput. Chem.* **2001**, *22*, 985. (b) Borras-Almenar, J. J.; Clemente-Juan, J. M.; Coronado, E.; Tsukerblat, B. S. *Inorg. Chem.* **1999**, *38*, 6081.